Numerical Modeling of Three-Dimensional Flows in Turbofan Engine Exhaust Nozzles

Stanley F. Birch* and Gerald C. Paynter†
Boeing Aerospace Company, Seattle, Wash.
and
D. B. Spalding‡ and D. G. Tatchell§
Concentration, Heat and Momentum, Ltd., London, England

An experimental and numerical study was conducted to investigate the use of three-dimensional viscous analysis for the design of internal mixers for jet noise suppression. Three flows, a full-scale free mixer, a full-scale lobed mixer, and a model-scale lobed mixer, were selected for study. Details of the experiments, turbulence modeling, and the determination of initial flow properties from engine operating properties are described together with a discussion of the usefulness of the analysis for mixing design. Overall the results are encouraging and, at least for the flows considered here, numerical analysis appears to compare favorably with model-scale tests as a simulation of the full-scale flow.

Nomenclature

C_1, C_2, C_D	= constants in turbulence model
D	= nozzle exit diameter
G	= turbulence generation
$\hat{h}$	= stagnation enthalpy
k	= turbulence energy
$\bar{P}$	= mean static pressure in a θr plane
PA	= ambient static pressure
PT_F	= total pressure, fan stream
PT_P	= total pressure, primary stream
R	= gas constant
r, R	= radial coordinate
R_0	= duct radius at nozzle exit
T	= static temperature
TT_F	= total temperature, fan stream
TT_P	= total temperature, primary stream
u	= velocity component in θ direction
v	= velocity component in radial direction
VI_F	= ideal velocity, fan stream
VI_P	= ideal velocity, primary stream
w	= velocity component in axial direction
Z	= axial coordinate
ϵ	= volumetric turbulence dissipation
θ	= angular coordinate
κ	= von Karman's constant
μ	= laminar viscosity
ρ	= density
σ	= Prandtl/Schmidt number
ϕ	= a general dependent variable

Introduction

INTERNAL mixing of the hot primary and the cooler secondary flows in a turbofan engine is a means of reducing jet noise through a reduction in the maximum nozzle exit velocity. By shaping as well as mixing, jet noise reduction greater than that resulting from a fully mixed flow can be achieved.[1] Many types of devices can be used to achieve internal mixing or nozzle exit velocity profile shaping for jet noise suppression. Among these devices are lobed mixers, vortex generators, combinations of vortex generators and mixers, and flow inverters. The use of a lobed mixer for jet suppression is illustrated in Fig. 1. The lobed mixer is the most successful of these devices to date and is typical of these devices, in that a larger number of geometric parameters can influence the nozzle exit velocity distribution.

The traditional design approach for such devices has been to test at model scale for a parametric variation of the important geometric parameters, select several promising configurations, and test these configurations at full scale to make a final selection and to validate the model-scale selection process. For a lobed mixer, for example, the lobe number, shape, inner and outer penetration, and the fan and primary inflow angles all have a strong influence on the nozzle exit velocity distribution. Since an exact model-scale simulation of the full-scale flow and hardware is seldom practical, full-scale results may deviate substantially from those expected from model testing. Because of these difficulties with the traditional design approach, it was decided to investigate the use of analysis as a possible substitute for testing. Clearly, if analysis of the three-dimensional compressible viscous flow proved adequate, it would be possible to replace some testing with analysis.

To accomplish this a three-dimensional compressible viscous flow analysis, based on the procedure of Patankar

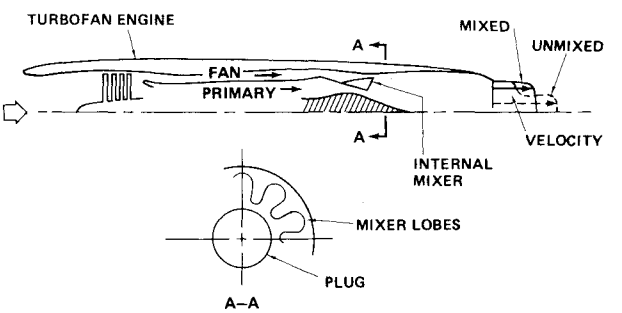

Fig. 1 Internal mixing for exhaust profile shaping.

Presented as Paper 77-204 at the AIAA 15th Aerospace Sciences Meeting, Los Angeles, Calif., Jan. 24-26, 1977; submitted March 8, 1977; revision received Feb. 21, 1978.

Index categories: Computational Methods; Nozzle and Channel Flows.

*Research Specialist.
†Research Specialist. Member AIAA.
‡Managing Director.
§Technical Manager.

and Spalding,[2] was selected and modified for application to internal mixing flows, and the required full-scale and model-scale flow data were gathered. Areas of concern were the adequacy of the numerics, the turbulence model, and the determination of initial flow properties from the known engine operating conditions. Could flow properties required to start the calculation be determined satisfactorily from information normally available to the designer?

To be meaningful, it was felt that evaluation of the analysis had to be based on a "prediction" rather than a "post-diction" of the results. To accomplish this arrangements were made with Concentration, Heat and Momentum, Ltd. (CHAM) to analyze the flow without prior knowledge of the flow results, using initial conditions supplied by Boeing. The results presented in this paper are the outcome of this work.

Experiments

Three flows were selected for investigation. These flows were a full-scale free mixer, a full-scale 12-lobe forced mixer, and a model-scale 12-lobe forced mixer. The free mixer is simply the unmodified engine fitted with a tail pipe which allows the fan and primary streams to mix freely downstream of the engine splitter plate (see Fig. 2). The lobed mixer cases were selected because of the relevance of these configurations as jet noise suppression devices, the three dimensionality of the flow, and as a means of investigating scale effects. The free mixer case was selected to check that the same analysis could be used in a two-dimensional flow and to establish the sensitivity of the predictions to initial turbulence intensity and swirl. A later discovery, that this flow was not two-dimensional (discussed in more detail under Results and Discussion), invalidated the detailed comparisons of predictions and measurements for this flow, but did not affect the utility of the study of the sensitivity of the predictions to the assumed initial conditions.

Full-scale tests were conducted at Boeing's propulsion and acoustic static test facility at Boardman, Ore. Flow was provided by JT8D turbofan engine. Total flow through the engine was measured using a calibrated bellmouth as an engine inlet. Fan and primary stream total pressures and temperatures were obtained using standard engine instrumentation. A photograph of the full-scale lobed mixer and a drawing of its location within the tail pipe are shown in Fig. 3.

For the full-scale lobed mixer, nozzle exit total pressures and temperatures were taken with a rotating rake. The rotating rake had 20 pairs of total pressure and temperature probes spaced at 0.8 in. out to 15.6 in. from the center of rotation. Data were taken in circumferential increments of 5 deg. Total velocity was calculated assuming that the local static pressure was equal to ambient static pressure.

For the full-scale free mixer case, flow surveys were taken at two circumferential clock positions with a traversing probe, which gave local total pressure, total temperature, swirl, and static pressure. Nozzle exit flow measurements were also made with the rotating rake described earlier. Axial and circumferential traversing probe locations are shown in Fig. 2.

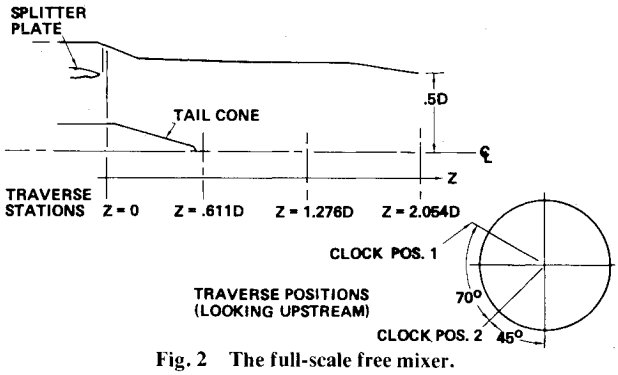

Fig. 2 The full-scale free mixer.

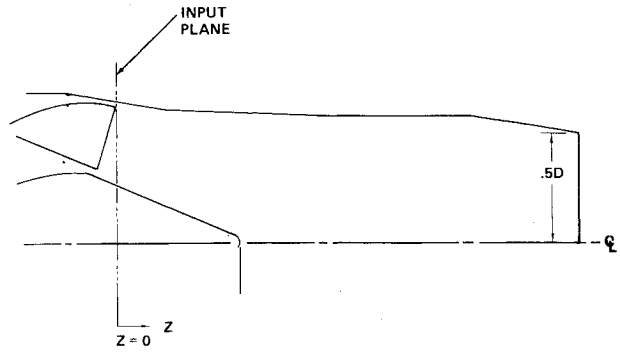

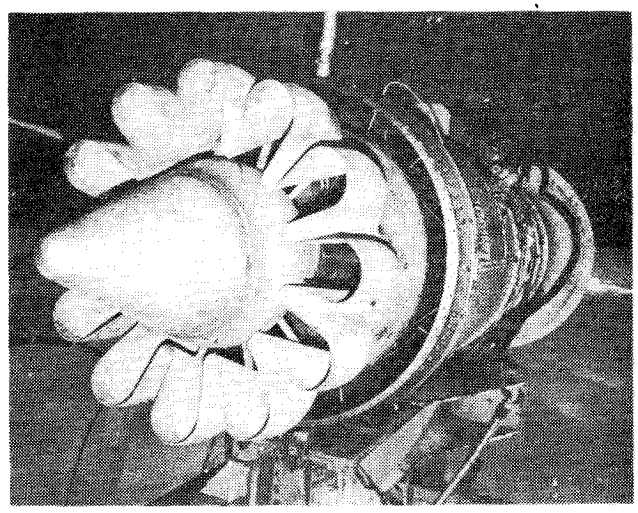

Fig. 3 Full-scale forced mixer.

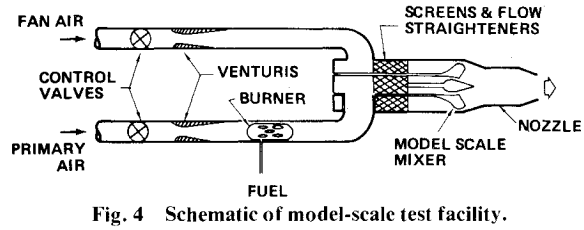

Fig. 4 Schematic of model-scale test facility.

Model-scale tests were conducted at Boeing's Propulsion Laboratory Thrust Vector Rig Number Two, located at North Boeing Field in Seattle, Wash. The test setup is shown schematically in Fig. 4. Airflow through the model fan and primary flow systems is controlled independently with hydraulically actuated control valves. The airflow rates through each system were measured with critical flow venturi meters. The primary airflow system was equipped with a burner which could produce primary total temperatures over 1000°F. Because the model-scale fan systems was not equipped with a burner, a model-scale simulation of the full-scale engine consisted of matching full-scale total pressures in both streams, but in simulating only the fan to primary total temperature ratio.

For the model-scale lobed mixer case, nozzle exit total pressures and total temperatures were measured with a rotating rake system similar to that used in the full-scale tests. The model-scale rotating rake had 10 pairs of total pressure and total temperature probes spaced at 0.25 in. radially to a radius of 2.5 in. Data were taken in circumferential increments of 4 deg. Velocity was again computed assuming that the local static pressure was equal to the ambient static pressure in the nozzle exit plane.

The model-scale mixer test hardware and flow simulation are typical of those used in the model-scale parametric testing or mixer configurations. It was 0.15 scale, but exact geometric similarity was not maintained between the model- and full-scale geometry. For example, model- and full-scale plug dimensions and the material thickness (scaled) were somewhat different. In addition, no attempt was made to simulate the asymmetry, swirl, flow obstructions, or the boundary-layer development of the full-scale flow. In both the model- and full-scale tests, the mass fluxes and total pressures in the primary streams were approximately equal to those in the fan streams. The pressure ratio, flow total pressure to ambient static pressure, was 1.8 for all of the tests.

Equations of Motion

For a three-dimensional compressible parabolic flow, the conservation equations can be written in cylindrical coordinates in the following general form:

$$\frac{1}{r}\frac{\partial}{\partial\theta}(\rho u\phi)+\frac{1}{r}\frac{\partial}{\partial r}(\rho rv\phi)+\frac{\partial}{\partial z}(\rho w\phi)$$
$$=\frac{1}{r}\frac{\partial}{\partial r}\left(r\Gamma_\phi\frac{\partial\phi}{\partial r}\right)+\frac{1}{r^2}\frac{\partial}{\partial\theta}\left(\Gamma_\phi\frac{\partial\phi}{\partial\theta}\right)+S_\phi$$

where u, v, and w are the velocity components in the θ, r, and z directions, respectively, ϕ is a general dependent variable, and Γ_ϕ and S_ϕ are its associated diffusion coefficient and source terms. The density is calculated from the ideal gas law

$$\rho=\bar{P}/RT$$

where R is the gas constant and is equal to 1716 ft^2/s^2-°R, and T is the temperature in degrees Rankine. The pressure $\bar{P}$ is the mean pressure in the θr plane.

Six equations of this form are solved in the present program: three for the velocity components, one for the stagnation enthalpy, and two for local turbulence quantities required to determine the effective turbulence viscosity μ_t. The diffusion coefficients Γ_ϕ for the velocity components and the stagnation enthalpy are evaluated as follows:

for u,v, and w: $\Gamma_\phi=\mu_{\text{eff}}=\mu_t+\mu$

for $\hat{h}$: $\Gamma_\phi=\mu_t/\sigma_{\hat{h}}+\mu/\sigma$

where μ_t and μ are the turbulent and laminar viscosities, $\sigma_{\hat{h}}$ is the turbulent Prandtl number, and σ is the laminar Prandtl number, taken here as unity. The corresponding source terms are given in Table 1. Note the distinction between P, the local pressure, and $\bar{P}$ the mean static pressure in the θr plane.

In addition it is necessary to satisfy the continuity equation which, in cylindrical coordinates, can be written as

$$\frac{1}{r}\frac{\partial}{\partial\theta}(\rho u)+\frac{1}{r}\frac{\partial}{\partial r}(r\rho v)+\frac{\partial}{\partial z}(\rho w)=0$$

Turbulence Model

In the present program the effective turbulent viscosity is calculated using a two-equation turbulence model, which involves solving partial differential equations for the turbulence energy k and its volumetric rate of dissipation ϵ. The equations are

$$\frac{1}{r}\frac{\partial}{\partial\theta}(\rho uk)+\frac{1}{r}\frac{\partial}{\partial r}(\rho rvk)+\frac{\partial}{\partial z}(\rho wk)=$$
$$\frac{1}{r}\frac{\partial}{\partial r}\left[r\left(\frac{\mu_t}{\sigma_k}+\mu\right)\frac{\partial k}{\partial r}\right]+\frac{1}{r^2}\frac{\partial}{\partial\theta}\left[\left(\frac{\mu_t}{\sigma_k}+\mu\right)\frac{\partial k}{\partial\theta}\right]+G-\rho\epsilon$$

Table 1 Source terms of the conservation equations

ϕ	S_ϕ
u	$-\frac{1}{r}\frac{\partial p}{\partial\theta}+\frac{\mu_{\text{eff}}}{r}\frac{\partial u}{\partial r}-\mu_{\text{eff}}\frac{u}{r^2}-\frac{1}{r}\frac{\partial}{\partial r}(\mu_{\text{eff}}u)-\frac{\rho uv}{r}$ $+\frac{\mu_{\text{eff}}}{r^2}\frac{\partial v}{\partial\theta}+\frac{1}{r^2}\frac{\partial}{\partial\theta}\left(\mu_{\text{eff}}\frac{\partial u}{\partial\theta}\right)+\frac{1}{r}\frac{\partial}{\partial r}\left(\mu_{\text{eff}}\frac{\partial v}{\partial\theta}\right)$ $+\frac{2}{r^2}\frac{\partial}{\partial\theta}(\mu_{\text{eff}}v)$
v	$-\frac{\partial p}{\partial r}+\frac{1}{r}\frac{\partial}{\partial r}\left(r\mu_{\text{eff}}\frac{\partial v}{\partial r}\right)-\frac{2\mu_{\text{eff}}v}{r^2}+\frac{\rho u^2}{r}$ $\mp\frac{1}{r}\frac{\partial}{\partial\theta}\left(\mu_{\text{eff}}\frac{\partial u}{\partial r}\right)-\frac{1}{r^2}\frac{\partial}{\partial\theta}(\mu_{\text{eff}}u)\frac{-2\mu_{\text{eff}}}{r^2}\frac{\partial u}{\partial\theta}$
w	$-\partial\bar{p}/\partial z$
$\hat{h}$	0

and

$$\frac{1}{r}\frac{\partial}{\partial\theta}(\rho u\epsilon)+\frac{1}{r}\frac{\partial}{\partial r}(\rho rv\epsilon)+\frac{\partial}{\partial z}(\rho w\epsilon)=$$
$$\frac{1}{r}\frac{\partial}{\partial r}\left[r\left(\frac{\mu_t}{\sigma_\epsilon}+\mu\right)\frac{\partial\epsilon}{\partial r}\right]+\frac{1}{r^2}\frac{\partial}{\partial\theta}\left[\left(\frac{\mu_t}{\sigma_\epsilon}+\mu\right)\frac{\partial\epsilon}{\partial\theta}\right]$$
$$+C_1\frac{\epsilon G}{k}-C_2\frac{\rho\epsilon^2}{k}$$

where

$$G\equiv\mu_t\left[2\left\{\left(\frac{\partial v}{\partial r}\right)^2+\left(\frac{1}{r}\frac{\partial u}{\partial\theta}+\frac{v}{r}\right)^2\right\}+\left\{r\frac{\partial}{\partial r}\left(\frac{u}{r}\right)+\frac{1}{r}\frac{\partial v}{\partial\theta}\right\}^2\right.$$
$$\left.+\left(\frac{1}{r}\frac{\partial w}{\partial\theta}\right)^2+\left(\frac{\partial w}{\partial r}\right)^2\right]$$

and

$$k=\tfrac{1}{2}(\overline{u'^2}+\overline{v'^2}+\overline{w'^2})$$

The turbulent viscosity μ_t is given by $\mu_t=C_D\rho k^2/\epsilon$. The constants appearing in the preceding equations are $\sigma_k=1.0$, $\sigma_\epsilon=1.3$, $C_1=1.44$, $C_2=1.92$, and $C_D=0.09$. A turbulence model of this form was first proposed by Harlow and Nakayama.[3] The specific version used here, developed by Launder and associates, is discussed in detail in Ref. 4.

It is known that this turbulence model will underpredict the mixing in planar flows for wakes and wakelike jets. Some of the constants must also be adjusted if both axisymmetric and planar jets are to predicted accurately.[4] Since the constants appropriate for planar flows were used in the present calculations, an overprediction of the spreading rate is to be expected for axisymmetric jets. For axisymmetric wakes or wakelike jets these effects tend to cancel.

Although the flowfield considered here is in general three dimensional, downstream of the mixer and within the tail pipe much of the mixing takes place in regions of the flow that locally approximate axisymmetric wakes or axisymmetric wakelike jets. Therefore, at least for the specific flows considered here, the selected turbulence model was expected to be adequate.

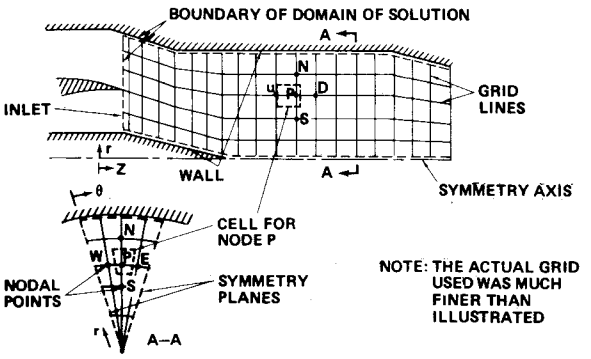

Fig. 5 Illustration of the solution domain and the finite-difference grid arrangement.

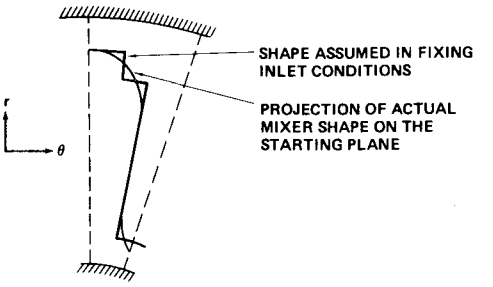

Fig. 6 The computational fit to the lobed mixer.

Boundary Conditions

The solution domain is shown outlined with the dashed line in Fig. 5. The conditions applied at the boundaries are as follows: at the inlet plane the values of u,v,w,p,k,ϵ, and the fluid temperature T are specified. The values used are discussed later. At the symmetry axis and the planes of symmetry, the velocity normal to the boundary is zero, and the flux of all other quantities across the boundary is zero. At the walls, the velocities are zero, and the rate of heat transfer is zero; one-dimensional turbulent wall functions, based on the familiar logarithmic wall law, are used to evaluate the wall shear stress and to provide boundary conditions on k and ϵ in the manner described by Launder and Spalding.[4]

Solution Method

The solution method employed is based on the finite-difference procedure of Patankar and Spalding.[2] The method as originally described was formulated in Cartesian coordinates. The version employed here represents an extension of the original method to handle cylindrical coordinates. The main features of the method are as follows:

1) The domain of solution is imagined to be covered by a three-dimensional lattice of grid lines, as shown in Fig. 5.

2) Finite-difference equations are derived for each of the dependent variables, by integrating the appropriate governing differential equation over a small control volume or cell surrounding each nodal point of the grid. These equations relate the value of the variable in question at a typical grid node P (see Fig. 5) to the values at the four neighboring nodes in the θr plane (N, S, E, and W), and to the value at the node immediately upstream (u).

3) Because the downstream value D is absent from the finite-difference equation at P (this is a feature of equations of the parabolic type), it is possible to perform calculations without any reference to values downstream of the plane in question. Solution may therefore be achieved by a marching integration which proceeds systematically downstream from the inlet plane to the end of the calculation domain. Each θr plane is visited in turn; at each the finite-difference equations are solved by an alternating-direction version of the familiar tridiagonal matrix algorithm (TDMA).

4) A novelty of the Patankar-Spalding method is the guess-and-correct procedure used to adjust the pressures. The practice at each axial plane is to first solve the u and v equations using "estimated" values of pressure. The estimate is usually based on the calculated values immediately upstream. The pressures are then corrected in such a way as to cause the corrected u and v velocities to satisfy local continuity. This is done by formulating and solving a set of finite-difference equations for the "pressure-corrections." These equations, it turns out, are of the same form as the finite-difference equations for the other variables and are solved by the same alternating-direction TDMA method.

5) The mean pressure at each axial station is deduced in a similar manner to that just described; thus, the axial velocities w are first calculated for an estimated value of P, which is subsequently corrected so that the implied values of axial velocity and density satisfy overall continuity for the duct section in question.

The grid employed in these calculations had 12 nodes in the radial direction and 8 in the circumferential direction. The grid nodes, which were approximately equally spaced in both directions, were arranged so that the boundaries of the computational finite-difference cells coincided, as far as possible, with the walls of the lobed mixer. At curved surfaces an exact correspondence was not possible so that the lobe shape assumed in the calculations did differ slightly from the actual shape. The areas of the fan and primary streams were, however, correctly simulated. This is illustrated in Fig. 6.

Determination of Initial Conditions

Simple Splitter

Of the six cases run (see Table 2), the first three were for the simple splitter. The initial conditions for these cases were based on experimental data from total pressure and total temperature traverses taken just downstream of the splitter, combined with the assumption that the flow was axisymmetric. The initial distributions of the three velocity components, the static pressure, and the static temperature used for the first two cases are shown in Fig. 7. Input for these cases differed only in the turbulence intensity specified for the primary core flow; 2% in the first core and 5% in the second. The third case was similar to the first, except that the swirl component was set to zero. The turbulence intensity in the fan stream, for all three cases, was assumed to be similar to that in a fully developed plane channel flow.

The initial turbulence dissipation rate was calculated using the formula

$$\epsilon = C_D^{3/4}(k^{3/2}/l)$$

The turbulence length scale l was set to a constant value in each stream, equal to 0.05 times the typical width of the stream, except close to the wall where l was set equal to κy, where y is the distance from the nearest wall and $\kappa = 0.42$. This procedure was used for all six test cases.

Lobed Mixers

Since detailed experimental data were not available for the flow at the mixer exit, an attempt was made to select a set of

Table 2 Initial conditions for swirl and turbulence intensity

	Simple splitter Full scale			Lobed mixer Full scale		Lobed mixer Model scale
Case	1	2	3	4	5	6
Swirl	Yes	Yes	No	No	No	No
Turb intensity, %						
Primary stream	2	5	2	5	5	5
Fan stream	Same as a fully developed channel flow			2	2	2

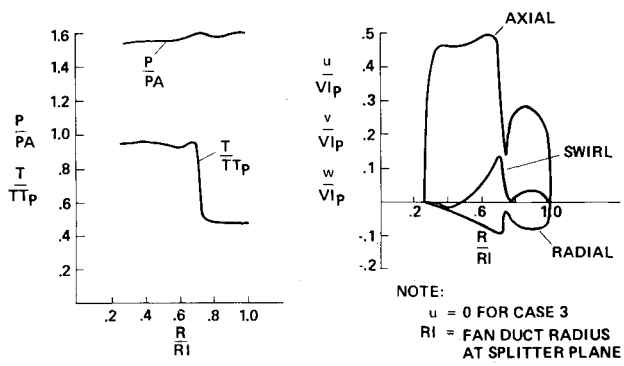

Fig. 7 Radial distribution of initial flow properties for cases 1, 2, and 3.

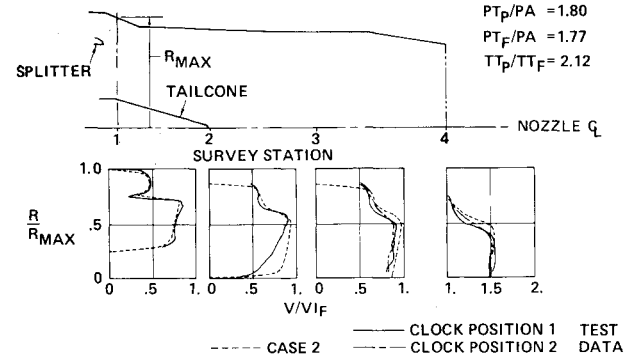

Fig. 8 Comparison between test data and analysis for the radial distribution of total velocity for free mixer.

initial conditions which was as simple as possible, consistent with the known integral properties of the flow. The calculations were started at a plane normal to the nozzle axis and just downstream of the mixer. The lobe geometry was projected onto this plane in such a way that the correct area split between the fan and primary streams was maintained.

At the initial station a basic distribution of the flow variables was selected for both the fan and the primary streams and later modified to account for wall boundary-layer effects. In the fan stream the total temperatures, the static pressure, and the axial velocity were assumed to be constant, with the radial velocity component selected to align the flow with the walls at the inner and outer boundaries and to vary linearly in between. A similar procedure was used for the primary stream. This flow was assumed to be axial except close to the plug (approximately 10% of the lobe height) where the flow direction was varied so that it would align with the wall at the plug surface. A corresponding radial static pressure gradient was also specified in this region.

The axial velocity at the near-wall grid nodes was then reduced to account for wall boundary-layer displacement effects. For cases 4 and 6, the displacement thickness was assumed to be uniform on all solid surfaces. For case 5 the displacement thickness in the primary stream on the central plug was assumed to be approximately four times that on the other surfaces. Case 5 with the nonuniform boundary-layer distribution was thought to best simulate the full-scale flow. Case 4 was included to provide information as to the effect of the initial boundary-layer specification on the mixing process. The overall displacement effect was calculated from the experimentally determined discharge coefficients of the fan and primary streams. The same initial turbulence intensity distribution was used for all three lobed mixer calculations; uniform values of 2% in the fan streams and 5% in the primary streams.

Results and Discussion

Full-Scale Results, Simpler Splitter

Differences in the initial turbulence level and swirl were found to have almost no effect on the predicted total velocity or total temperatures at the nozzle exit for the first three cases. A comparison between the predicted and measured velocity profiles for case 2 is shown in Fig. 8. Radial traverses were taken at four axial stations between the splitter and the nozzle exit planes. Overall agreement between the test data and the predictions is fair. However, the predicted radial distribution of velocity at the second axial station, near the end of the engine tail cone, is poor. This discrepancy appears to be due to an underprediction of the local static pressure near the center of the tail pipe. Farther downstream, where the static pressure in a plane is approximately constant, predicted and measured velocity profiles are in good agreement, except for the location of the mixing layer. The

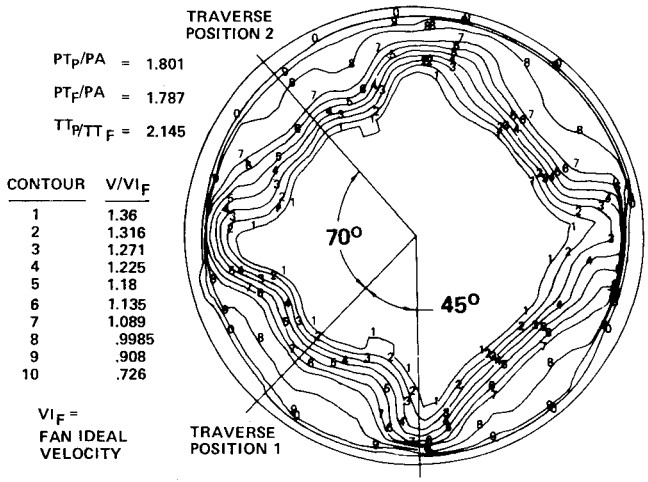

Fig. 9 Contour map of the nozzle exit velocity distribution from test of the full-scale free mixer.

predicted location of the mixing layer between the fan and primary streams is displaced radially outward about 7% of the local duct radius, compared with the experimental data.

Initially this was very puzzling. At that time only the traverse data were available, and the two traverses at the nozzle exit seemed to confirm the expected symmetry of the flow. This suggested that the discrepancy was due to some deficiency in either the numerical algorithm or the turbulence model. Yet, a detailed study of both indicated nothing which could account for the discrepancy. The problem was eventually resolved when, in a later test, a rotating rake was used to map the velocity field at the nozzle exit of a similar engine. The results are shown in Fig. 9, and the radial traverse locations from the earlier test are noted on the map. The contour map clearly shows the strong asymmetry. But, since the earlier traverse stations were inadvertently located across "flats" in the contour map, they gave no indication of this except for the displacement of the mixing layer.

It is now known from later tests that the asymmetry of this flow is due to the swirling primary stream interacting with four large engine struts located just downstream of the turbine exit. The resulting secondary flow, which appears to be a pair of counter-rotating circulating cells in each quadrant, leads to a progressive distortion of the flow as it travels downstream. A consenquence of this is a change in the sign of the swirl toward the outer edge of the duct, which would be impossible if the flow was axisymmetric. This was measured in the earlier test, but its significance was not appreciated at that time. Consequently a comparison between the predicted and measured swirl is of limited interest and is not presented here.

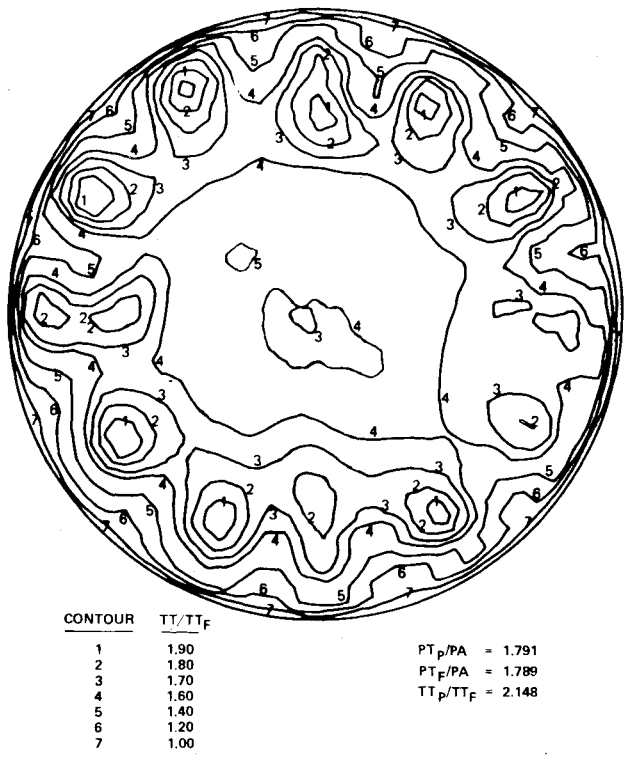

Fig. 10 Nozzle exit total temperature map from test of the full-scale forced mixer.

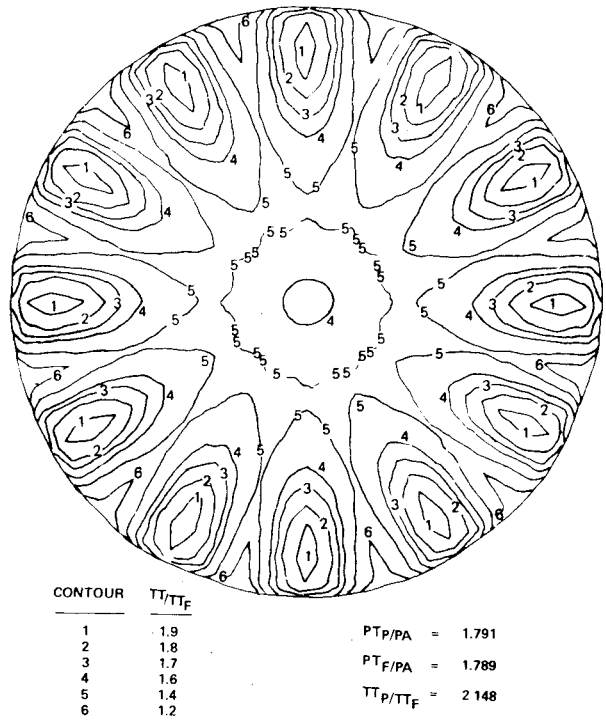

Fig. 12 Computed nozzle exit total temperature map for the full-scale mixer, case 5.

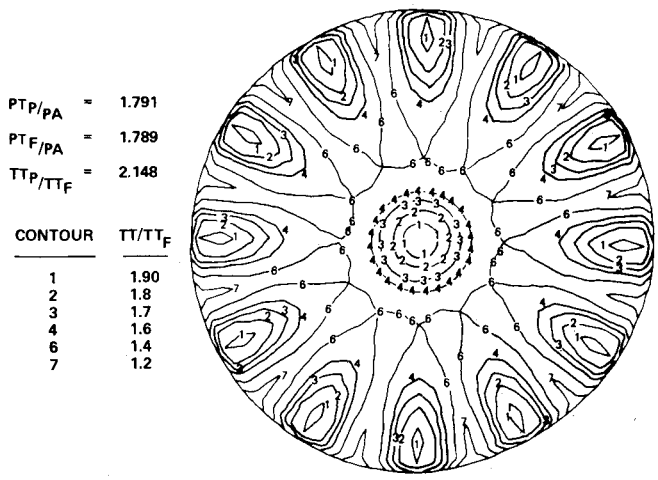

Fig. 11 Computed nozzle exit total temperature map for the full-scale mixer, case 4.

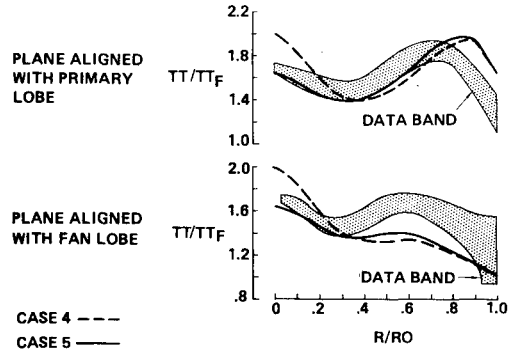

Fig. 13 Measured and predicted radial distribution of total temperature at nozzle exit for the full-scale forced mixer.

In retrospect, it is clear that the actual flow was substantially different from that assumed in the analysis, and a comparison of the measured and predicted results is only of limited use as a test of the validity of the analysis. It is believed, however, that the observed insensitivity of the predictions to the initial swirl and/or turbulence intensity does have some general validity.

Full-Scale Results, Lobed Mixer

A contour map of the total temperature distribution at the nozzle exit plane from the experimental test of the full-scale forced mixer is given in Fig. 10. Since the mean total pressures of the fan and primary streams are almost equal for this particular engine, the total pressure distribution outside the wall boundary layers is very uniform and, therefore, is not presented here. A further consequence of this uniformity in total pressure is the qualitative similarity of the total temperature and total velocity contour maps. The discussion here will be limited to the total temperature data.

The total temperature map shows considerable asymmetry, and it should perhaps be mentioned that the fan and primary flows at the upstream entrance of the lobed mixer were essentially identical to the fan and primary flows at the splitter plane of the free mixer flow. Thus, the swirl, initial boundary-layer development, and flow disturbances due to struts and instrumentation probes, noted for the free mixer flow, were also present for the full-scale lobed mixer flow. The passage of this flow through the mixer lobes undoubtedly led to strong secondary flows at the mixer exit plane. In the specification of initial conditions for the numerical calculations, no attempt was made to simulate these effects.

Contour maps of the total temperature at the nozzle exit plane for cases 4 and 5 are shown in Figs. 11 and 12. Apart from the circumferential irregularity of the actual flow, both calculations seem to predict the correct trend. As expected, case 5 is the better of the two predictions. Note that the predicted contours are generally more elliptical than the corresponding experimental contours. Measured and predicted total temperatures, in planes aligned with the fan and primary lobes, are shown in Fig. 13. The radial locations of the total temperature peaks appear to be about right for

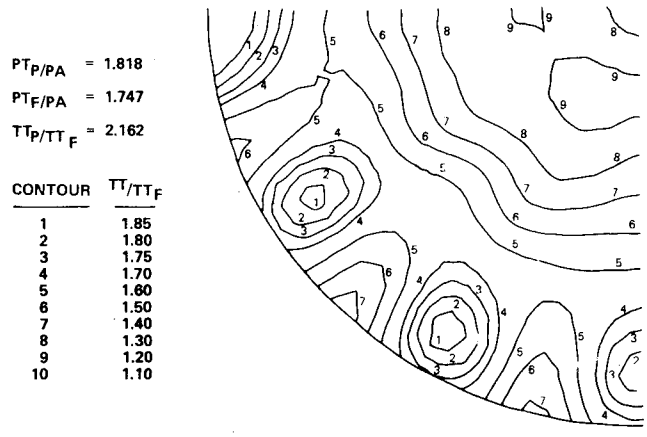

Fig. 14 Nozzle exit total temperature map from model-scale test of the forced mixer.

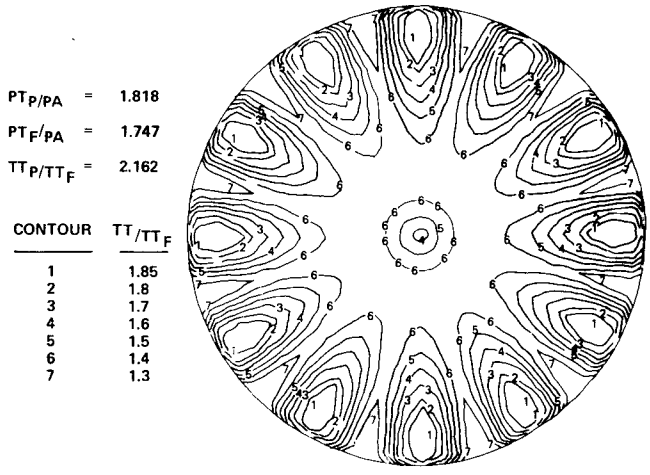

Fig. 15 Computed nozzle exit total temperature map for the model-scale forced mixer, case 6.

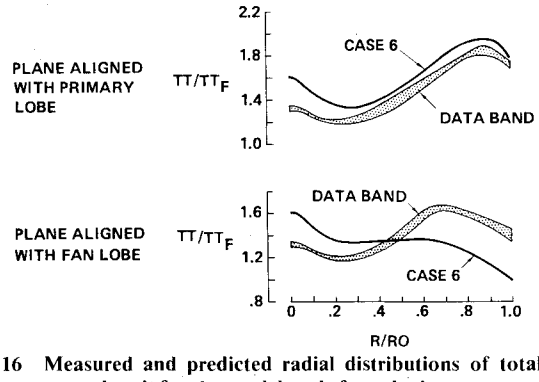

Fig. 16 Measured and predicted radial distributions of total temperature at nozzle exit for the model-scale forced mixer.

case 5 and too far out for case 4. The total temperature distribution near the center of the nozzle is also much better in case 5. Since the only difference between cases 4 and 5 is in the specification of the initial boundary-layer distribution, it would seem that the predicted total temperature distribution at the nozzle exit plane can be quite sensitive to the specification of the initial boundary layer distribution at the mixer exit plane.

Model-Scale Results, Lobed Mixer

A contour map of the experimental total temperature distribution is shown in Fig. 14 for the model-scale lobed mixer. As described previously, flow obstructions and swirl known to be present full scale, were not simulated in the model-scale test, and the resulting flow at the nozzle exit is therefore less distorted.

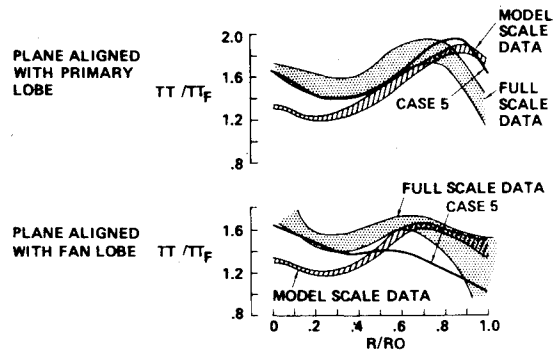

Fig. 17 Comparison of model- and full-scale radial total temperature distributions.

The corresponding total temperature predictions are shown in Fig. 15. Predicted contours are again more elliptical than the experimental contours. The total temperature at the center of the nozzle is also a little higher than the measured results. This seems to indicate that the assumed initial boundary-layer thickness on the plug surface was too small.

Comparison between the measured and predicted total temperatures, in planes aligned with the fan and primary lobes, are shown in Fig. 16. In line with the primary lobes, the case 6 predictions of total temperature are a little high, but overall the agreement is very good; between the lobes, the mixing is again underpredicted.

Comparison of Results

Comparisons between the nondimensional model and full-scale mixer results are shown in Fig. 17. The corresponding predictions for case 5 are shown in the same figure. In line with the primary lobes, predicted values of the total temperature are closer to the full-scale data than are the corresponding model-scale data. In line with the fan lobes, the predicted total temperature distribution is also better, except near the outer edge of the nozzle, where the predicted results fail to exhibit the rise in total temperature found experimentally. There is also a tendency, both model and full scale, for the total temperature contours downstream of the primary lobes to become approximately circular. This is not well predicted by the analysis and appears to be associated with the underprediction of total temperature between the primary lobes. This discrepancy is believed to be due to the characteristics of the turbulence model used, but, because of the uncertainty in initial conditions, no definite conclusion is possible.

On balance, it was felt that the analysis compared favorably with the model-scale results as a simulation of the full-scale flow, and that it was in some respects superior. Many, if not most, of the discrepancies between the model- and full-scale experimental results can be accounted for by differences in initial conditions, so that a better model-scale simulation could have been obtained, at least in principle. However, because of the cost involved, this is seldom practical.

As to the impact of the analysis on the design process, the analysis obviously has not eliminated either model- or full-scale testing. Use of the analysis has certainly led to a heightened awareness, on the part of the designer, to the sensitivity of the flow (for the particular device being designed) to the various geometric and flow parameters. It has also led to a much greater emphasis on defining local flow properties, especially at the start of the mixing region. Parametric analysis rather than parametric testing is being used to an ever increasing degree to define likely configurations. It is important to emphasize, however, that new applications of the analysis should be validated through comparisons with test data on a case by case basis.

Conclusions

The major conclusion of this study is that current numerical methods and turbulence models can be used for the prediction of certain complex three-dimensional viscous flows of practical importance. An accurate estimate of initial conditions, however, is important. Indeed, the data presented here have indicated that most substantial discrepancies between predictions and experimental data were probably due to a poor estimate of initial conditions. The first three test cases described here are examples of this. In these areas the discrepancy between predictions and experimental data appears to be almost wholly due to the incorrect assumption that the flow was axisymmetric. The sensitivity of the predictions, for the flow near the center of the tail pipe downstream of lobed mixers to the assumed boundary-layer thickness on the plug, suggests that certain features of flow at the input plane may have to be specified fairly accurately. It would be wrong to extrapolate from the results presented here to a general claim that three-dimensional viscous flows can now be accurately predicted. This is certainly not true. But many complex turbulent flows of practical importance can be predicted with acceptable accuracy. The present paper describes one carefully documented example of this.

References

[1]Crouch, R. W., Coughlin, C. L., and Paynter, G. C., "Nozzle Exit Flow Profile Shaping for Jet Noise Reduction," *Journal of Aircraft*, Vol. 14, Sept. 1977, pp. 860-867.

[2]Patankar, S. V. and Spalding, D. B., "A Calculation Procedure for Heat, Mass and Momentum Transfer in Three-Dimensional Parabolic Flows," *International Journal of Heat and Mass Transfer*, Vol. 15, Oct. 1972, pp. 1487-1806.

[3]Harlow, F. H. and Nakayama, P., "Transport of Turbulence Energy Decay Rate," Los Alamos Science Lab., Univ. of California, Rept. LA-3854, 1968.

[4]Launder, B. E. and Spalding, D. B., "The Numerical Computation of Turbulent Flows," *Computer Methods in Applied Mechanics and Engineering*, Vol. 3, March 1974, pp. 269-289.